THE SOUND GENERATED BY A TWO-DIMENSIONAL SHEAR LAYER: A COMPARISON OF DIRECT COMPUTATIONS AND ACOUSTIC ANALOGIES

Tim Colonius*
Sanjiva K. Lele†
Parviz Moin‡
Department of Mechanical Engineering
Stanford University, Stanford CA 94305

Abstract

The sound generated by vortex pairing in a two-dimensional mixing layer is studied by solving the Navier-Stokes equations (DNS) for the layer and a portion of its acoustic field, and by solving acoustic analogies with source terms determined from the DNS. Predictions for the acoustic field based on Lilley's equation are in excellent agreement with the DNS results giving detailed verification of Lilley's acoustic analogy for the first time. We show that parts of the full source term which arise when the left-hand-side of Lilley's equation is linearized should not be neglected solely because they are attributable to refraction and scattering, nor because they are proportional to the dilatation. Lilley's source, $-2u_{i,j}u_{j,k}u_{k,i}$, appears to be mainly responsible for the overall directivity of the acoustic field produced by the vortex pairings, which is highly focused at shallow angles to the streamwise axis. Scattering of the waves by the flow appears also to be significant, causing the directivity to be more omnidirectional than the Lilley source alone would predict. We also show how small errors in determining the sources, especially those due to scattering, can sometimes lead to large errors in the predictions.

1. Introduction

The sound generated by a two-dimensional compressible mixing layer is investigated using Direct Numerical Simulation (DNS) of the Navier-Stokes equations and by the solution of acoustic analogy equations. For turbulent shear flows, the rearrangement of the equations of motion leading to an acoustic analogy is ambiguous since the flows do not possess compact vorticity fields[1]. This ambiguity can be partially alleviated by performing asymptotic expansions of the disturbances to a parallel transversely sheared flow[2] which results in an acoustic analogy similar to the one proposed by Lilley[3]. Ultimately, however, nonlinear effects which dominate the flow preclude an unambiguous analytical solution of the asymptotic expansion. In general one must regard the source term as independently known, determined either by experiment or computational fluid dynamics, and it cannot be determined *a priori* how accurate is the estimate for the acoustic field thus produced.

As is discussed by Lighthill[4], computations of aerodynamic sound generation can be broadly divided into two strategies: (1) The computational domain includes only the near field without attempting to resolve the acoustic waves. Subsequently an acoustic analogy is solved with source terms that have been determined from the near field computations; (2) The computational domain includes the near field and, to a limited extent, the acoustic region. The acoustic field exterior to the computational boundary is deduced by solving the acoustic analogy given source terms determined from the near field, or by solving the wave equation given boundary data.

To date nearly all aeroacoustic computations involving turbulent shear flows have been computed using strategy (1), and Lighthill[4] appears to be a strong proponent of this strategy for low Mach number flows. We assert, however, that currently computations of this type are not completely reliable since the validity of the answer lies with the correctness of the acoustic analogy which, as discussed above, is not certain. Even if the acoustic analogy used is correct, it is possible that small computational errors in determining the sources can lead to large errors in the computed sound field, as we show by example below.

In strategy (2), the acoustic far field is solved directly from the basic equations of motion it can be compared with the acoustic field predicted by the acoustic analogy and thus the validity of the acoustic analogy can be directly assessed. We present such predictions for the sound generated by the pairing of vortices in a mixing layer. In

*Research Assistant, Member AIAA; Present position: Assistant Professor of Mechanical Engineering, California Institute of Technology, Pasadena, CA 91125
†Assistant Professor, Member AIAA, also with the Department of Aeronautics and Astronautics
‡Franklin & Caroline Johnson Professor of Engineering, Associate Fellow AIAA, also with the NASA-Ames Research Center

To be presented at the First Joint CEAS/AIAA Aeroacoustics Conference, Munich, Germany, June 12–15, 1995

our previous work, we have developed a numerical scheme for sound generation problems, and validated it on a number of model problems; see Colonius *et al.*[5,6,9,10], and Mitchell *et al.*[7,8] Our DNS results for the mixing layer were previously presented[5] – the results of that study are important to the current work we summarize them in Section 2. In Section 3 we derive several different forms of the acoustic analogy and discuss the predictions given source terms which have been computed using the DNS data. We note that due to space limitations, a great many specific details of our analysis are only mentioned briefly here, but will be given greater attention in a forthcoming publication.

2. DNS of the Mixing Layer

We summarize here the methodology and results from the DNS. The complete details of the numerical scheme are given by Colonius[10]. The 2D unsteady compressible Navier-Stokes equations plus conservations of mass and energy are solved numerically on a computational domain depicted in Figure 1. The Mach numbers of the high and low speed streams are $M_1 = 0.5$ and $M_2 = 0.25$, respectively. The temperature of the two streams is equal.

Note that in what follows all the streamwise and normal velocities u_1, and u_2 are normalized by the speed of sound far from the mixing region, a_∞. Lengths (x_1 and x_2) are normalized by the vorticity thickness of the layer at $x_1 = 0$. The density, ρ is normalized by its value far from the mixing region, ρ_∞, and the pressure, p, is normalized by ρa_∞^2.

Since the Mach number is low and the temperature of the streams is equal, we model the fluid as a perfect gas with constant viscosity and conductivity. The Reynolds number based on the vorticity thickness and velocity of the high speed stream is 1000. The ratio of specific heats, γ, is 1.4.

A Cartesian grid of 2300 by 847 grid points in the x_1 and x_2 directions, respectively, is used. The grid in x_1 is uniform with spacing $\Delta x_1 = 0.15$ in the "physical" domain, up to $x_1 = 285$. A uniform grid spacing of $\Delta x_2 = 0.15$ is used in a region near $x_2 = 0$. The grid transitions to a uniform but coarser spacing of $\Delta x_2 = 0.80$. for large $\pm x_2$. The time step, Δt, was 0.0567, well below the CFL limit for the current scheme.

One major problem in aeroacoustic computations is the posing of boundary conditions. "Non-reflecting" boundary conditions have been developed extensively for wave equations[11], and to a more limited extent, for the linearized Euler equations (see, for example, Giles[12]). In our previous work [9] we modified Giles' boundary conditions to apply them to viscous flows which contain shear. While linear boundary conditions are sufficiently accurate for acoustic waves exiting the computational domain, the accuracy of the boundary conditions at the outflow boundary where large scale non-acoustic flow structures must pass is poor. In fact we showed[9] that by introducing a "sponge outflow" region can greatly reduce spurious reflections over the linear boundary conditions alone. The technique utilizes a region just upstream of the downstream boundary where a combination of grid stretching and low-pass filtering to greatly reduce the amplitudes of fluctuations before they hit the outflow boundary. Since the least-resolved disturbances in a finite differenced flow can propagate upstream it is possible that the solution will become contaminated with small wavelength disturbances from the sponge. Also, grid stretching itself produces reflected acoustic waves which propagate both upstream and downstream in the flow. In several test[9], both of these effects caused reflections which about 3 orders of magnitude smaller than the spurious reflections which were created by the linear boundary condition alone.

In order to study the sound generated by large scale structures in the mixing layer, the layer is forced at its most unstable frequency, f, and its first three subharmonics, $f/2$, $f/4$, and $f/8$, respectively. This causes the layer to roll up and pair at stationary positions in space, and allows the sound generated by the mixing layer to be investigated without the additional complication of fine grained turbulence. The layer becomes approximately periodic in time as far downstream as the end of the of the computational domain[5] (disincluding the sponge region).

In terms of the generated acoustic field, this has the important consequence of causing the acoustic sources to be stationary, as it is in the experiments of Laufer & Yen[13], Bridges and Hussain[14] and others. The frequency content of the flow can be determined by discrete Fourier Transforms (DFT) over a relatively short period of time. In the case of random forcing it would be necessary to ensemble average over many realizations with much greater computational expense.

The computations are forced at the inflow with eigenfunctions from linear stability analysis:

$$g(x_1, x_2, t) = \tilde{g}(x_2) e^{2\pi i(\alpha x_1 - \omega t)}, \qquad (1)$$

where g is any of u_1, u_2, ρ or p. $\tilde{g}$ is the complex eigenfunction, which we normalize for each frequency such that its maximum streamwise

component is 0.001, α is the complex wavenumber whose real part is 0.131,0.0635,0.0309, and 0.0152 and whose imaginary part is -0.0193,-0.0145,-0.0085,and -0.0045 for frequencies f,$f/2$,$f/4$, and $f/8$ respectively. ω is the real frequency equal to 0.0501,0.0251,0.0125, and 0.00627 for frequencies f,$f/2$,$f/4$, and $f/8$ respectively. The phase of the subharmonics is chosen to minimize the distances between the pairings.

The instantaneous vorticity field at $t = 68T$, where $T = 1/f$, is shown in Figure 2 and plainly shows the roll up and two subsequent pairings of the layer. Note that the third subharmonic frequency does not cause a third pairing within the computational domain. The instability waves saturates near where the roll-up and pairings take place, at locations $x_1 \approx 50$, 75, and 175 for the f, $f/2$ and $f/4$) respectively.

Turning our attention now to the acoustic field away from the region near $x_2 = 0$, we choose the dilatation as the acoustic variable in the DNS for reasons outlined in ref. 10. The dilatation is directly related to the acoustic pressure for large x_2 by conservation of mass:

$$\frac{\partial p'}{\partial t} + M_1 \frac{\partial p'}{\partial x_1} = -\gamma \frac{\partial u_i}{\partial x_i} \tag{2}$$

(and with (2) with M_1 replaced by M_2 for large $-x_2$. Isocontours of the DFT of the dilatation for the fundamental and first two subharmonic frequencies is plotted in Figure 3. The contours are not shown in the near field region (small x_2) since the dilatation there is not purely acoustic. Note that the saturation locations for the instability waves are indicated on the plots with tick marks on the x_1 axis. The acoustic waves at the $f/2$ and $f/4$ apparently emanate from the region where the instability waves at those frequencies saturate. That is, the acoustic waves at the subharmonics appear to emanate from the regions where the pairings occur. This is similar to the other analytical and experimental observations[13,15]. In fact, it appears that the waves are primarily focused downstream, reaching their maximum amplitude near the $+x_1$ axis. Unlike the experiments, however, the acoustic field at f has maximum amplitude in directions nearly normal to the layer and the waves appear to emanate from a region upstream of the saturation location and very near the inflow boundary. We believe that these waves are an artifact of the instability wave forcing at the inlet. Though great care was taken to impose the inlet forcing in a way which did not excite an incoming acoustic wave, approximations in the nonreflecting boundary conditions used at the inflow make it impossible to entirely eliminate any spurious incoming acoustic wave entirely. The amplitude of the acoustic waves shown in Figure 3(a) is roughly 5000 times smaller than the amplitude of the inlet forcing, indicating that the error is very small indeed. Apparently any sound at frequency f generated by the flow itself is at a smaller level. It also appears that some contamination from the inlet forcing may also be present at $f/2$ and $f/4$ where waves emanating from a region very near the inflow boundary can also be seen. These waves are of of comparable magnitude as those emanating near the inflow at the fundamental frequency but are, in the case of the subharmonics, smaller than those waves which are produced by the pairings.

As was discussed in our previous work[5], the acoustic field at the *unforced* frequencies appears to be seriously contaminated by waves produced downstream of the physical domain, i.e. in the sponge outflow region. Evidently the sound generated by the flow within the physical part of the domain is very much smaller for the unforced frequencies, and so small errors from the sponge overwelm the acoustic field. The presence of these spurious waves emanating from the sponge and the spurious waves due to the inlet forcing indicate the need for further refinements to the nonreflecting boundary conditions.

3. Prediction of the Acoustic Field Based on Solution of the Acoustic Analogy

In testing the acoustic analogy, we pass over Lighthill's equation and proceed directly to Lilley's equation since many investigators[3,2,16,17] have noted that when there is a mean flow certain effects which are lumped together in the Lighthill source term should ideally be retained on the left-hand-side (the wave propagation operator) of the acoustic analogy. When the mean flow contains shear a generalization of the acoustic analogy due to Lilley[3] is:

$$\begin{aligned} D_t\left(D_t^2\Pi - (a^2\Pi_{,j})_{,j}\right) + 2u_{k,j}(a^2\Pi_{,j})_{,k} \\ = -2u_{i,j}u_{j,k}u_{k,i}, \end{aligned} \tag{3}$$

where D_t is the convective derivative, $\frac{\partial}{\partial t} + u_k \frac{\partial}{\partial x_k}$, Π is the logarithmic pressure defined by $\Pi = \frac{1}{\gamma} \ln p$, and we have used Cartesian tensor notation with the shorthand that the subscript after the comma refers to differentiation with respect to that coordinate direction. Like Lighthill's equation, Equation (3) is an exact consequence of the basic conservation principles but is a single nonlinear equations in 4 variables and therefore cannot be solved uniquely.

Often the flow is well approximated by a steady parallel transversely sheared flow (i.e one for which $u_2 = 0$ and u_1 is only a function of x_2, which we denote $U(x_2)$, Π and ρ are constants) plus fluctuations, which we denote with a prime. Using this decomposition in ((3)) gives:

$$\begin{aligned}\bar{D}_t\left(\bar{D}_t^2\Pi' - \Pi'_{,jj}\right) + 2U_{,2}\Pi'_{,12} = \Gamma(x_1,x_2,t) = \\ \bar{D}_t\Big(\underbrace{(u_i'u_j')_{,ij}}_{\text{Ia}} - \underbrace{u'_{i,i}u'_{j,j}}_{\text{IIa}} + \underbrace{(a^{2'}\Pi')_{,j}}_{\text{IIIa}} \\ + \underbrace{a^2\Pi'_{,i}\Pi'_{,i}}_{\text{IVa}} + \underbrace{\Pi'_{,j}u_i'u'_{j,i} + u_j'(u_i'\Pi'_{,i})_{,j}}_{\text{Va}}\Big) - \\ 2U_{,2}\Big(\underbrace{(u_2'u_j')_{,1j}}_{\text{Ib}} - \underbrace{u'_{2,1}u'_{j,j}}_{\text{IIb}} + \underbrace{(a^{2'}\Pi'_{,2})_{,1}}_{\text{IIIb}} \\ + \underbrace{a^2\Pi'_{,1}\Pi'_{,2}}_{\text{IVb}} + \underbrace{\Pi'_{,1}u_2'u'_{j,j} + u_j'(u_2'\Pi'_{,j})_{,1}}_{\text{Vb}}\Big)\end{aligned} \tag{4}$$

where $\bar{D}_t$ indicates the convective derivative *following the parallel flow* , $\bar{D}_t = \frac{\partial}{\partial t} + U(x_2)\frac{\partial}{\partial x_1}$. Note that no a^2 term appears on the left-hand-side since by the current nondimnensionalization the value of a^2 for the parallel transversely sheared flow is 1.

The linear terms in Equation (4) now only contain the logarithmic pressure fluctuation when the fluctuations are small the right-hand-side vanishes it reduces to the Pridmore-Brown equation for fluctuations in a parallel transeversely sheared flow. The products of fluctuations on the right hand side, then, truly represent the sources of sound in a parallel transversely sheared flow, and for that case there is no longer any ambiguity associated with the acoustic analogy approach – it is consistent with a perturbation expansion of the basic flow equations. Unfortunately, the mean of real turbulent shear flows is neither parallel nor solely transversely sheared since the flow spreads and certain refraction effects are still lumped into the right-hand-side source rather than explicitly accounted for in the propagation operator. Therefore we still regard (4) as an acoustic analogy, and note that it is still an exact equation. Note that in what follows we choose $U(x_2)$ to be the initial velocity profile at $x_1 = 0$ from the DNS. Other choices are possible, but we defer considering them to a future paper. Note that the equation is exact regardless of how $U(x_2)$ is chosen–the choice simply causes a different split between the terms on the right and left hand sides.

We digress from our discussion of the acoustic analogy to summarize our solution procedure for numerically solving (4) when the right hand side is computed from the DNS results of the last section. Since the coefficients on the left-hand-side are no longer a function of x_1 or t, we solve (4) by taking the Fourier transform with respect to x_1 and t.

Equation (4) is discretized over a finite period of time, $\mathcal{T}$, such that $t_j = \frac{\mathcal{T}j}{N}$, for $j = 0, 1, \cdots, N-1$ where N is the number of samples. We leave x_1 in continuous form, and thus define the Fourier transformed pressure perturbation, P_n as:

$$P_n(k,y) = \frac{1}{N}\sum_{j=0}^{N-1}\int_{-\infty}^{+\infty}\Pi' e^{-2\pi i(kx_1 + jn/N)}dx_1, \tag{5}$$

Fourier transforming (4) and defining a new variable ϕ_n such that $P_n(k,x_2) = (\omega_n + Uk)\phi_n(k,x_2)$ we obtain:

$$\phi_n'' + \lambda_n^2(k,x_2)\phi_n = -\frac{G_n(k,x_2)}{2\pi i(\omega_n + Uk)^2}, \tag{6}$$

where the prime now denotes differentiation with respect to x_2, G_n is the Fourier transform (in x_1 and t) of the source term Γ and where

$$\begin{aligned}\lambda_n^2 = &\left[4\pi^2\left((\omega_n + Uk)^2 - k^2\right)\right] \\ &- \left[(\omega_n + Uk)((\omega_n + Uk)^{-1})''\right],\end{aligned} \tag{7}$$

where $\omega_n = n/\mathcal{T}$.

We solve (6) numerically by mapping the infinte domain in x_2 to a finite one and using fourth order finite differences for the derivatives – the resulting pentadiagonal system of equations is directly inverted. The full details of the scheme and its validation are given in ref. 10.

The numerical solution of (6) requires that the source term Γ be discrete-transformed in t and continuous Fourier transformed in x_1. Since Γ will only be known on a discrete grid, we compute the Fourier transform in x_1 via numerical quadrature (as opposed to a DFT) so that periodicity in x_1 is not assumed. Thus we approximate:

$$\begin{aligned}G_n(k,x_2) &= \int_{-\infty}^{\infty}\hat{\Gamma}_n(x_1,x_2)e^{2\pi ikx_1}dx_1 \\ &\approx \sum_{l=1}^{N_x} w_l\hat{\Gamma}_n(x_1^{(l)},x_2)e^{2\pi ikx_1^{(l)}},\end{aligned} \tag{8}$$

where $\hat{\Gamma}_n(x_1,x_2)$ is the DFT (in time) of Γ, and $x_1^{(l)}$ are the discrete values of x_1 between appropriate limits on which the source is non-zero, and w_l are the weights for a particular quadrature scheme. Since the transform need only be performed for values of k between $-\omega_n/(1+M_2)$ and $\omega_n/(1-M_1)$ the exponential factors in the quadruture do not oscillate too rapidly to obtain an accurate solution and we use Simpson's rule for the quadrature,

defined on the node points of the Navier-Stokes solution. Note that if the source does not become negligibly small for large x_1, then the series (8) must be truncated at a finite point. It turns out that the sources terms do not decay to zero within the physical part of the computational domain but that there is a rapid decay of the source terms in the sponge, and we make use of that fact in computing the integral Fourier transform in x_1. The justification for this is that the decay of the source source terms in the sponge region is sufficiently slow such that the Fourier transform in x_1 over the range $-\omega_n/(1+M_2) < k < \omega_n/(1-M_1)$ is not seriously affected. A more detailed justification of this will be included in a forthcoming publication.

Even if the integral transform or the sponge were not used, a similar problem would arise in solving the acoustic analogy since *the source terms are simply not known downstream of the computational boundary.*

Given P_n, the inverse transform in x_1 is performed to obtain the dilatation at discrete frequencies:

$$\hat{\Theta}_n = \int_{-\omega_n/(1+M_2)}^{\omega_n/(1-M_1)} (\omega_n + Uk)^2 P_n(k, x_2) e^{2\pi i k x_1} dk, \tag{9}$$

where the infinite limits on the integration have been replaced by $-\omega_n/(1+M_2)$ and $\omega_n/(1-M_1)$, since for larger values of k, P_n decays exponentially in $\pm x_2$ (i.e. λ_n^2 is negative). For small values of x_1, and x_2 this integral can be performed with numerical quadrature in an analogous manner to (8). For large values of x_1 and x_2 the exponential factors oscillate too rapidly for an accurate solution and in that case we approximate the integral in (9) analytically using the method of stationary phase. The details of the integration are given in ref. 10.

One part of the solution method which turns out to be very sensitive to small computational errors is the DFT in time of the acoustic source term Γ. Because the layer is not prefectly periodic in time, the DFT (computed in the standard way) contains some errors due to very low frequency components which cannot be resolved. In particular, these errors cause "leakage" in the low frequency components of the transform. We have developed a technique, which will be discussed in detail in a forthcoming paper, which attempts to remove these aperiodic low frequency components from the signal. It works by computing the DFT over a large number of overlapping segments of the data, where the data over the segment is first made periodic by subtracting out a linear trend between the first and last data points of the segment. Then by averaging the large number of segments, a DFT relatively free from the low frequency aperiodic contamination is obtained. Note that the technique is not equivalent to common windowing techniques (see, for example, Press *et al.*[18]) all of which attempt to *resolve* the aperiodic components into their nearest discrete frequency bins. Figure 4(a) and (b) shows the predicted acoustic field at frequency $f/2$ where the DFT of the source Γ has been computed in 2 different ways: (a) the standard DFT with a period of 64T and (b) our technique which attempts to remove the low frequency aperiodic components. Note that while the DFT gives an acoustic which does not agree at all with the DNS (Figure 3(b)) – it is more than an order of magnitude too large and appears to emanate primarily from downstream of the second pairing and in the sponge. In contrast, our DFT technique produces an acoustic field in excellent agreement with the DNS (a more quantitative comparison is given below). Finally, note that the source terms themselves (before solution of the acoustic analogy) differ by only a very small ($< 5\%$) amount at frequency $f/2$, while the resulting acoustic fields differ by more an order of magnitude. In what follows, therefore, we use our DFT technique to compute the acoustic source terms.

Figure 4(b) and (c) shows the predicted acoustic field at $f/2$ for full source term, Γ, and term I only (by term I we mean term Ia and Ib combined), respectively. The figure shows that the two predictions are nearly identical. This is an important conclusion since Goldstein[2,16] has argued that the terms Ia and Ib alone should be sufficient to predict the sound at low Mach numbers. Goldstein presents two essentially distinct arguments for why this is the case. First, in terms of the acoustic analogy approach, he argues[16] that terms II, III, IV, and V should be small because (1) some of the terms are proportional to the dilatation in the flow which is very small compared to term I for low Mach numbers, and (2) some terms appear because of linearization of the left-hand-side of (3) and should therefore be considered as the effects of scattering and refraction (which might be supposed to be of only secondary importance). Second, in terms of a perturbation expansion of the flow about "first order" solutions to (4) (i.e solutions for which the source, Γ, is set to zero), Goldstein[2] shows that term V, being a triple product of the first order solutions can be neglected as a higher order effect, and that the *sum* of terms II and IV only produces changes to Π' in the far field which are proportional to Π'^2, i.e. they are again

a higher order effect. Finally, term III contains the fluctuating sound speed and should therefore only be important when temperature variations in the flow are large.

We now show that the first rationale (that terms II to V are small because they represent scattering/refraction and/or are proportional to the dilatation) is not strictly correct. The acoustic field at $f/2$ resulting from terms II through V individually is shown in Figure 5. Terms IIb, IVa, and IVb can be seen to produce acoustic fields *of comparable magnitude* to the total source Γ. Now since term IIb is neglected because it is proportional to the dilatation and term IV is neglected on refraction/scattering grounds they should be negligible individually. In fact, as we show below term I of Γ itself contains terms which are proportional to the dilatation and which represent refraction and scattering, but which, nevertheless, generate non-negligible acoustic fields, even though the Mach number of the present flow is small. Finally, term III appears to be negligible on its own, which is not surprising given that we are considering a low Mach number flow which has the same temperature in both streams.

The bottom line is that apparently terms II, III, IV, and V can be dropped outright from the acoustic source term *but only when terms II and IV are taken in combination.* This should serve as an important warning to investigators who are tempted to through out terms proportional to the dilatation on the grounds that they are small. We note that the same conclusions can be drawn for the source term at $f/4$ though we have not included those results here for the sake of brevity.

Comparing Figure 3 to Figure 4(b) or (c) we see that there is an excellent qualititaive agreement between the acoustic analogy predictions with source Γ and the DNS. The results are replotted in Figure 6 with the magnitude of the dilation shown along arcs at various distances from the saturation point for the instability wave corresponding to the particular frequency plotted, i.e. $x_1 = 75$ for $f/2$ and $x_1 = 175$ for $f/4$. The angle θ of the observation point is defined from the $+x_1$ axis. We pick the saturation point as the "apparent origin" of the waves. Note that we do not compare the DNS and the Acoustic Analogy in the near field (for $|x_2| < 40.0$ in the plots) since the dilatation from the DNS is not purely acoustic there. Quantitatively the agreement remarkably good at most of the locations. Note that the data is plotted on a linear scale. One significant exception is at very large angles (i.e. near the inflow boundary) for the first subharmonic frequency where as argued above some spurious waves are being generated by the inflow boundary condition. These waves do not appear in the acoustic analogy prediction since they have no significant impact on the source terms.

We now examine term I of Γ alone in more detail. Figure 5(i) and (j) shows the acoustic field at $f/2$ for terms Ia and Ib individually. It is very striking how very little the acoustic field for either either term Ia or Ib alone resembles the acoustic field for their sum. Both have a magnitude significantly larger than the their sum and show very large contributions coming from the region near the second pairing which evidently nearly cancel altogether from the sum, the sum very clearly coming dominately from the region near the first pairing. The fact that terms Ia and Ib have such a significant cancellation between them suggests that there is perhaps a better way to express the sum of the two terms.

Note that the form of the source terms on the right-hand-side is not unique. One can use the basic equations of motion to re-express the terms in different forms. One possibility is to carry the convective derivative $\bar{D}_t$ through the differentiations with respect to x_i and x_j in term Ia. Performing this and using the basic equations of motion to rewrite term I we obtain:

$$\bar{D}_t(\bar{D}_t^2\Pi' - \Pi'_{,jj}) + 2U_{,2}\Pi'_{,12} = \Gamma_2 = \underbrace{-2u_{i,j}u_{j,k}u_{k,i}}_{\text{A}} \underbrace{- u'_k(a^2\Pi'_{,j})_{,jk}}_{\text{B}} \underbrace{- 2u'_{j,k}(a^2\Pi'_{,k})_{,j}}_{\text{C}}, \tag{10}$$

plus a number of additional terms which are similar to terms II through V of Γ, and which similarly sum to give very little contribution to the acoustic field. The new source, Γ_2, contains the original Lilley source (see (3)) plus two terms which arise from the linearization of the second two terms on the left-hand-side of (3), Note they are similar to the second two terms on the left-hand-side of (4), but contain the fluctuating velocity rather than the parallel transversely sheared velocity, $U(x_2)$. Thus we believe that these two terms should be considered as due to scattering and refraction as are other terms resulting from the left-hand-side linearization.

Now considering the magnitude of the three terms of Γ_2. Source A is very much smaller than the sum of terms B and C, since term A is actually proportional to the dilatation in a two-dimensional flow – in the present case it is over two orders of magnitude smaller. However, the acoustic field produced by term A and by the sum of terms B and C, as is depicted in Figure 5(k),(l), and (m), have comparable magnitude.

Clearly terms B and C must undergo a very much greater degree of cancellation in the acoustic analogy solution than does term A, and evidently the most energetic part of the motions contributing to terms B and C does not contribute to the acoustic field. This makes sense if terms B and C represent refraction/scattering, since then the contribution to the total product would then be the acoustic part of the pressure times the total fluctuating velocity. Once again, because the cancellation is so great, small computational errors have the potential to ruin the prediction. As we discussed above in connection with taking the DFT of the source terms, very small errors due to low frequency aperiodic components of the signal can produce large errors in the acoustic prediction. In fact these errors are traceable to terms B and C of Γ_2, while term A is much less sensitive to the DFT process. This stresses the need to move as many of scattering/refraction terms to the left-hand-side of the acoustic analogy as is possible.

In Figure 7 we plot asymptotic far field (using the method of stationary phase to evaluete (9)) for both the term A alone, and the acoustic field from the total source Γ_2, for both $f/4$ and $f/2$. Indeed it appears that the effect of terms B and C is simply to redistribute the acoustic waves to a more omnidirectional distribution as we would expect scattering to do. Also, the directivity becomes increasingly oscillatory and in fact, the overal directivity resembles very closely the directivity for the scattered waves which results when a plane wave interacts with a vortex, see for example Figure 5 of Colonius *et. al.*[6]. The directivity from term A alone, while very highly focused at shallow angles to the $+x_1$ axis, is not as "superdirective" as the sources of Crighton & Huerre[15]. It is of interest to speculate on what effect three dimensionality would have on the above analysis. For 3D flow, the Lilley source term (term A) is, of course, no longer proportional to the dilatation in the flow. It seems feasible that term A will then become relatively more important than B and C and thus be the primary source in a 3D flow.

4. Summary and Conclusions

The sound generated by vortex pairing in a two dimensional mixing layer has been investigated by solving the Navier-Stokes equations directly (DNS) for the near field and a portion of the acoustic field, and by solving acoustic analogies with source terms determined from the DNS. Predictions based on Lilley's[3] acoustic analogy, with the source term written in form proposed by Goldstein[2], are in excellent agreement with the DNS results. Thus a detailed verification of Lilley's acoustic analogy applied to shear flow with a noncompact vorticity field has been achieved for the first time. The good agreement between the acoustic analogy and the DNS at the first and second subharmonic frequencies is achieved even though: (1) the acoustic field is some 4-5 orders of magnitude smaller than the near field fluctuations, (2) there is a very significant amount of cancellation in the source terms, especially those attributable to scattering of the waves, and (3) that some spurious waves are generated by the boundary conditions - especially at the fundamental frequency and at frequencies which are unforced. Apparently the "true" acoustic field at those frequencies is very much smaller than the first and second subharmonics in the present flow. Further improvements to the accuracy of nonreflecting boundary conditions are clearly warranted.

Several terms which result from the linearization of the left-hand-side of Equation (3) are found to produce negligible acoustic fields. The standard arguments for their neglect - because they represent scattering of the sound or that they are proportional to the dilatation, and are therefore of secondary importance at low Mach numbers appear to be incorrect, since these terms individually produce significant acoustic fields. Instead, certain terms can be neglected because they can be shown to be equivalent to higher order terms in an asymptotic expansion of the disturbances in a parallel transversely sheared flow. The most significant part of the source term is actually Lilley's term $-2u_{i,j}u_{j,k}u_{k,i}$ which appears to be responsible for the overall directivity of the acoustic field by the vortex pairings. This directivity is highly focused at shallow angles to the streamwise axis. Even at the relatively low Mach number of the mixing layer, scattering of the waves by the flow appears to be significant, causing the directivity to be more omnidirectional than the Lilley source alone would predict.

Acknowledgments

This work has been sponsored by the Office of Naval Research, grant N00014-92-J-1626, and computer time and support has been provided by the NASA Ames Research Center and the Center for Turbulence Research.

References

[1]Kambe, T. 'Acoustic emissions by vortex motions.' *J. Fluid Mech.*, **173**, pp. 643–666, 1986.

[2]Goldstein, M.E. 'Aeroacoustics of turbulent shear flows.' *Ann. Rev. Fluid Mech.*, **16**, pp. 263–285, 1984.

[3]Lilley, G.M. 'On the noise from jets' *AGARD CP-131.* 345 pp.

[4]Lighthill, M.J. 'Report on the final panel discussion on computational aeroacoustics' ICASE Report No. 92-53, 1992.

[5]Colonius, T., Lele, S.K. & Moin, P. 'Direct computation of the sound generated by a two dimensional shear layer.' AIAA paper 93–4328, 1993.

[6]Colonius, T., Lele, S.K. & Moin, P. 'The scattering of sound waves by a vortex — numerical simulations and analytical solutions.' *J. Fluid Mech.*, **26**e, pp. 271–298, 1994.

[7] Mitchell, B.E., Lele, S.K. & Moin, P. 'Direct Computation of the Sound Generated by Vortex Pairing in an Axisymmetric Jet.' AIAA paper 95–0504, 1995.

[8]Mitchell, B.E., Lele, S.K. & Moin, P. 'Direct computation of the sound from a compressible co-rotating vortex pair.' *J. Fluid Mech.*, **285**, pp. 181–202, 1995.

[9]Colonius, T., Lele, S.K., & Moin, P. 'Boundary conditions for direct computation of aerodynamic sound generation.' *AIAA Journal*, **31**, pp. 1574–1582, 1993.

[10]Colonius, T. 'Direct Computation of Aerodynamic Sound' Ph.D. Thesis, Department of Mechanical Engineering, Stanford University, 1994.

[11]Givoli, D. 'Non-reflecting Boundary Conditions.' *J. Comput. Phys.*, **94**, pp. 1–29, 1991.

[12]Giles, M.B. 'Non-reflecting boundary conditions for Euler equation calculations.' *AIAA J.*, **28**, pp. 2050–2058, 1990.

[13]Laufer, J. & Yen, T. 'Noise generation by a low-Mach-number jet.' *J. Fluid Mech.*, **134**, pp. 1–31, 1982.

[14]Bridges, J. & Hussain, F. 'Direct evaluation of aeroacoustic theory in a jet.' *J. Fluid Mech.*, **24**e, pp. 469–501, 1992.

[15]Crighton, D.G. & Huerre, P. 'Shear-layer pressure fluctuations and superdirective acoustic sources.' *J. Fluid Mech*, **22**e, pp. 355–368, 1990.

[16]Goldstein, M.E. *Aeroacoustics*, McGraw-Hill, 1976.

[17]Phillips, O.M. 'On the generation of sound by super-sonic shear layers.' *J. Fluid Mech*, **9**, pp. 1–28, 1960.

[18]Press, W.H., Teukolsky, S.A., Vetterling, W.T., & Flannery, B.P. *Numerical Recipes in FORTRAN*, Cambridge University Press, 1992.

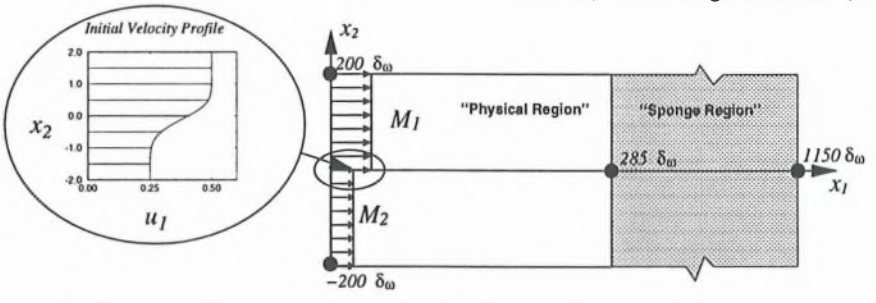

Figure 1. Schematic diagram of flow and computational domain.

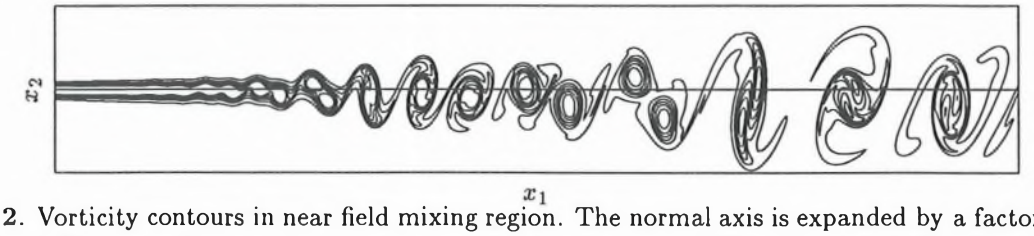

Figure 2. Vorticity contours in near field mixing region. The normal axis is expanded by a factor of 2.5. A portion of the computational domain is shown which extends to 285δ in the streamwise direction and $\pm 10\delta$ in the normal direction. Contour levels: Min: -0.13, Max: 0.01, Increment: 0.02.

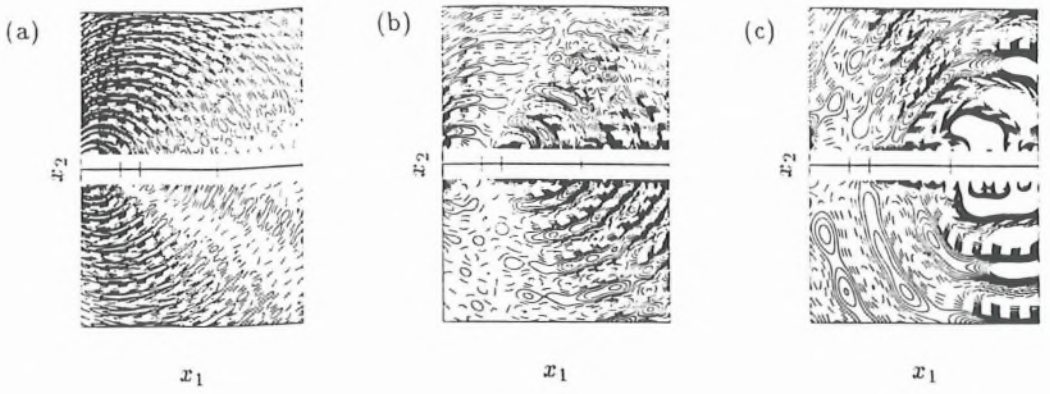

Figure 3. Contours of the real part of the DFT of the dilatation away from sheared region for frequencies f, $f/2$ and $f/4$. Note that the real part corresponds to the waves at a particular phase (or instant in time). The entire domain (except sponge) is shown. The approximate saturation locations for the fundamental frequency and its first two subharmonics are indicated on the plot with the tic marks on the x_1 axis at $x_1 = 50$, $x_1 = 75$ and $x_1 = 175$, respectively. Dashed lines are negative contours and solid lines are zero and positive contours. Contour levels (all times 10^6) – Plot (a): -0.2 to 0.2 at intervals of 0.02; Plot (b): -0.4 to 0.4 at intervals of 0.04; Plot (c): -1.0 to 1.0 at intervals of 0.1.

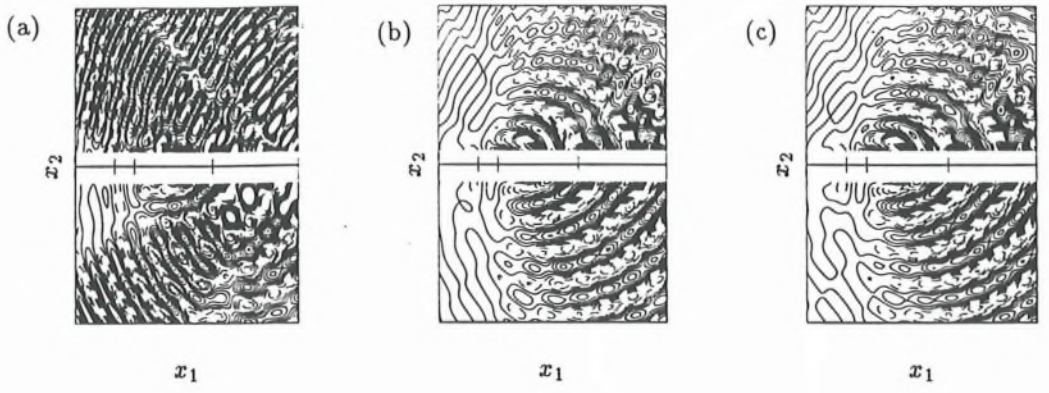

Figure 4. The acoustic field predicted by acoustic analogy (found by solving (4)). The real part of the DFT of the dilatation is plotted for frequency $f/2$. Plot (a) uses the full source term Γ with its DFT computed using the standard method; plot (b) uses the full source Γ with its DFT computed using our technique designed to remove aperiodic low frequency components from the signal as discussed in the text; plot (c) uses term I of Γ only with the new DFT technique. Contour levels for all plots (all times 10^6): -0.4 to 0.4 at intervals of 0.04.

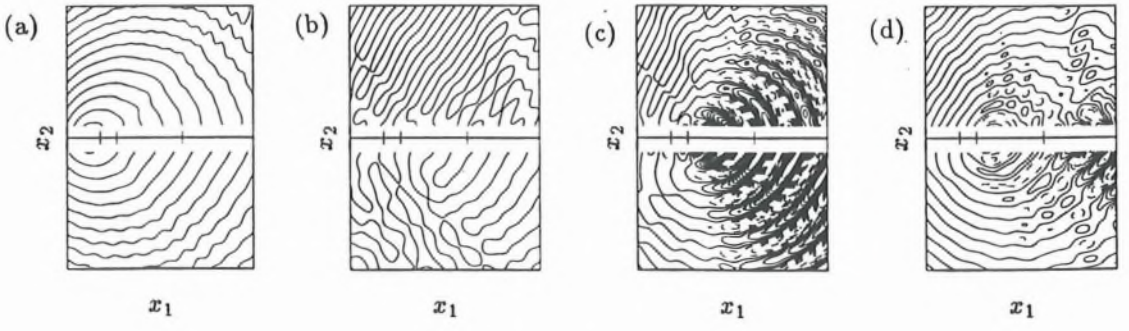

Figure 5. Continued on following page.

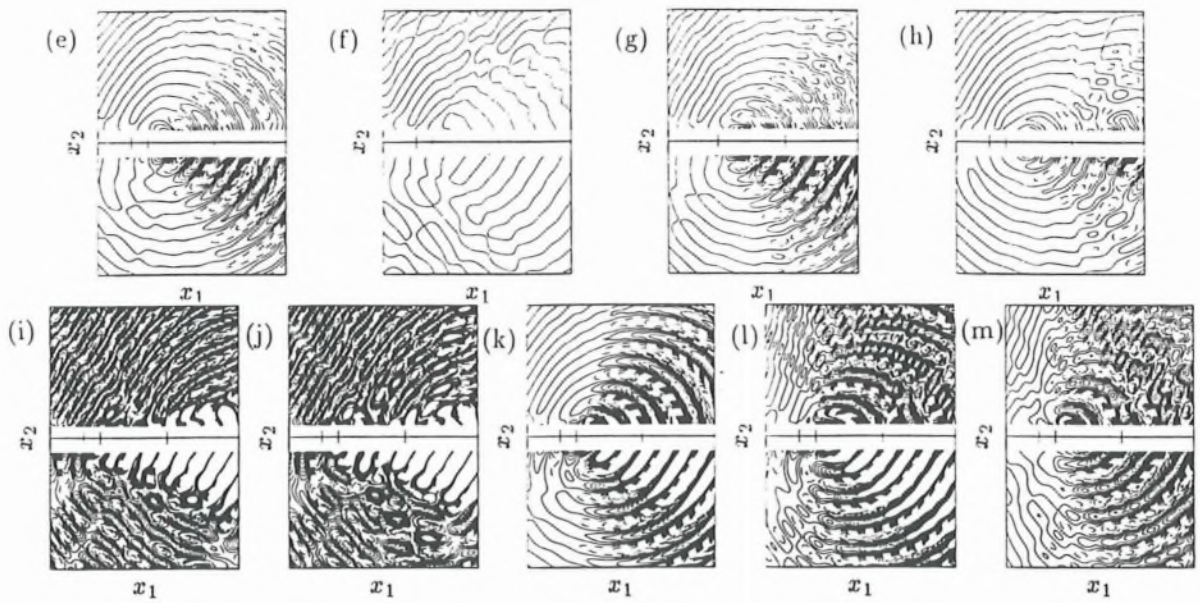

Figure 5. Predictions at frequency $f/2$ but with individual terms taken as the source (see Equation (4)). (a) IIa; (b) IIIa; (c) IVa; (d) Va; (e) IIb; (f) IIIb; (g) IVb; (h) Vb; (i) Ia; (j) Ib; (k) A ; (l) the sum of B and C; (m) all of Γ_2 (A+B+C) Contour levels for all plots (all times 10^6): -0.4 to 0.4 at intervals of 0.04.

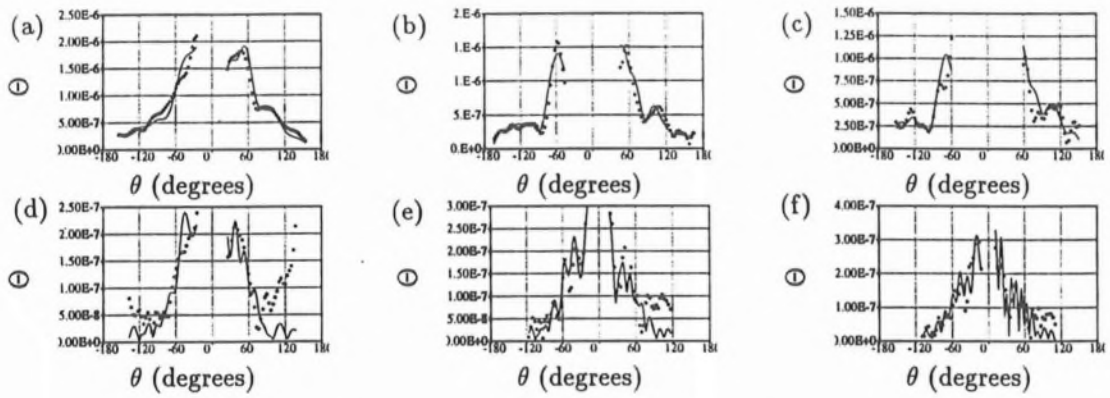

Figure 6. Comparison of dilatation – acoustic analogy (solid lines) vs. DNS (symbols), shown on arcs at different distances, r, from the apparent origin of the waves: (a) $f/4$, $r = 100.0$; (b) $f/4$, $r = 150.0$; (c) $f/4$, $r = 200.0$; (d) $f/2$, $r = 100.0$; (e) $f/2$, $r = 150.0$; (f) $f/2$, $r = 200.0$.

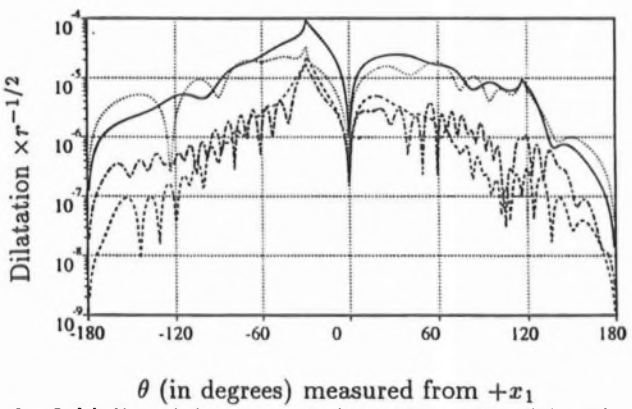

Figure 7. The asymptotic far field directivity computed from Equation (6) with source terms: —— Term A only at frequency $f/4$; ····· Full source Γ_2 at frequency $f/4$; - - - - Term A only at frequency $f/2$; —·— Full source Γ_2 at frequency $f/2$